JPCC-MgCl2.6EtOH-2011

DATASET · DECEMBER 2012

READS
56

9 AUTHORS, INCLUDING:

Thushara K S
Università degli Studi di Torino
15 PUBLICATIONS **95** CITATIONS
SEE PROFILE

Biswajit Saha
Sikkim Manipal Institute of Technology
12 PUBLICATIONS **41** CITATIONS
SEE PROFILE

Madhavan Chalat
University of British Columbia - Vancouver
16 PUBLICATIONS **188** CITATIONS
SEE PROFILE

THE JOURNAL OF PHYSICAL CHEMISTRY C

ARTICLE

pubs.acs.org/JPCC

Toward an Understanding of the Molecular Level Properties of Ziegler−Natta Catalyst Support with and without the Internal Electron Donor

K. S. Thushara,[†] Edwin S. Gnanakumar,[†] Renny Mathew,[‡] Ratnesh K. Jha,[†] T. G. Ajithkumar,[‡] P. R. Rajamohanan,[‡] Krishna Sarma,[§] Sudhakar Padmanabhan,[§] Sumit Bhaduri,*[,∥] and Chinnakonda S. Gopinath*[,†]

[†]Catalysis Division, National Chemical Laboratory, Dr. Homi Bhabha Road, Pune 411 008, India

[‡]Central NMR Facility, National Chemical Laboratory, Dr. Homi Bhabha Road, Pune 411 008, India

[§]RTG Vadodara Manufacturing Division, Research Centre, Reliance Industries Limited, Vadodara 391 346, Gujarat, India

[∥]Department of Chemistry, Northwestern University, Evanston, Illinois 60208-3113, United States

ABSTRACT: Two Ziegler−Natta catalysts supported on molecular adducts, namely, $MgCl_2 \cdot 6EtOH$ (ME) and $MgCl_2 \cdot 5EtOH \cdot EtOOCPh$ (Est-ME), have been prepared. A systematic effort has been made to unravel the molecular level structure−property relationships of the catalysts and adducts. Ethylbenzoate is an internal electron donor, and its in situ formation through EtOH + PhCOCl coupling is successfully achieved. The above adduct has been treated with $TiCl_4$, and the resultant catalyst (Ti/Est-ME) is evaluated for ethylene polymerization activity. IR and ^{13}C CP/MAS NMR of Est-ME (Ti/Est-ME) show carbonyl features at 1730 (1680) cm^{-1} and 169 (170) δ, respectively, providing direct support for the presence of ester as an integral part. In spite of low surface area, Ti/Est-ME gives higher yield for ethylene polymerization than the one derived from ME. The results indicate that electronic environment is more important than surface area or any other single factor in determining the polymerization activity.

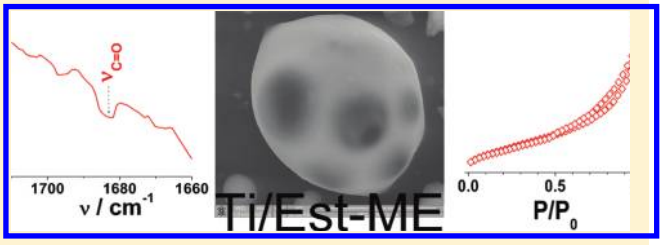

1. INTRODUCTION

$MgCl_2$-supported titanium catalysts for the polymerization of olefins have had spectacular success in simplifying the polymerization process and improving polymer quality. The basis for the development of the high-activity supported catalysts[1] lay in the discovery of "activated" $MgCl_2$ being able to support $TiCl_4$ and give high catalyst activity for both ethylene and propylene polymerization. After the name of the discoverers, these solid catalysts are usually referred to as Ziegler and Ziegler−Natta catalyst, respectively. In the mid-1970s, it was discovered that certain Lewis bases, when present as an integral part of the $MgCl_2$ support and/or when added from outside during polymerization, are capable of significantly increasing the stereospecificity of propylene polymerization. These Lewis bases, typically an ester or ether, are called electron donors (ED) and when incorporated in $MgCl_2$ as an integral part of the support are referred to as the internal electron donors (IED). They bind strongly to $MgCl_2$, and their basic function is to control the amount and distribution of $TiCl_4$ on the support.[2−12] In contrast, external electron donors (EED) are EDs that enhance stereospecificity in the presence of the correct IED and are added externally during the polymerization reaction. Although innumerable organic compounds have been tested as potential IEDs and EEDs, only a few combinations were found to give satisfactory results.

Understanding how the activated surface of magnesium chloride can influence the properties of the active sites has turned into a great challenge for the techniques of surface science, spectroscopy, and computational methods.[13−15] It is generally believed that the IED blocks particular sites on the $MgCl_2$ surface which otherwise, upon coordination with $TiCl_4$, would generate precursors of nonstereospecific active sites.[6,10,11] Spitz et al.[12] recently reported that IED might have no direct role in the active site formation; however, it stabilizes the $MgCl_2$ crystallites. One of the main reasons for this uncertainty regarding the role of IED is that the majority of the experimental information available in the literature comes mainly from detailed analysis of the microstructure of polypropylene, rather than the support and/or the catalyst itself. The difficulties in interpreting data from propylene polymerization experiments also arise from the fact that a widely used IED such as ethyl benzoate (EB) is eluted from $MgCl_2$-supported titanium catalyst under the general polymerization conditions. Furthermore, there is enough evidence to suggest that there are multiple modes of interactions between IED, EED, cocatalyst (alkyl aluminum complexes), and the active Ti-sites.[16−23] Thus, direct investigation of the active species on the catalyst is an extremely complex problem even if other difficulties such as complexity of the constitution, low content of the active sites in the

Received: August 18, 2010
Revised: December 8, 2010
Published: December 31, 2010

catalyst, and high sensitivity to oxygen and moisture in the ambient conditions are ignored.

The aim of the present paper is to understand the molecular level properties of the $MgCl_2 \cdot 6EtOH$ adduct (ME) and that of $MgCl_2$ with inbuilt IED, $MgCl_2 \cdot 5EtOH \cdot EtCOOPh$ (Est-ME), by subjecting them to structural, spectroscopy, microscopy, and textural analysis. Est-ME and its analogues are known to be highly effective as supports for the Ziegler−Natta catalyst and have many advantages over ME.[24] Until now, no literature reports are available on full spectroscopic characterization and structural properties of Est-ME. Therefore, detailed structural and spectroscopic studies of Est-ME and ME and a comparison between them are important toward a better understanding of the role of IED. We also report comparative data on the activities of Ziegler−Natta catalysts made by using these supports. The present report is a part of ongoing investigations from our group to understand the Ziegler−Natta catalysts and new molecular adducts.[25]

2. EXPERIMENTAL SECTION

2.1. Materials. In this work, Ziegler−Natta catalyst support materials were prepared by the azeotropic distillation method reported in our previous work.[25] $MgCl_2$ powder mesh (containing 5% H_2O), absolute ethanol 99.99%, titanium tetrachloride ($TiCl_4$), and triethylaluminum (TEAl) (all from Sigma−Aldrich) were used as received. Benzoyl chloride (BC), hexane, toluene, and chlorobenzene (Merck) were used as such. Ethylene (purity 99.9%) was taken from a commercial plant and used without further purification to make polyethylene.

2.2. Preparation of Molecular Adducts and Catalysts. 2.2.1. Ethanol Adduct (ME). The ME adduct was prepared by the azeotropic distillation method.[24,25] Partially hydrated $MgCl_2$ (0.1 M), absolute ethanol (2 M), and a required amount of toluene were refluxed in a 500 mL RB flask under continuous azeotropic distillation of water for 3 h. The above solution was cooled to and maintained at 0 °C until the crystallization was complete. Then, the crystalline solid was washed with *n*-hexane, dried, and stored in a vacuum desiccator.

2.2.2. Esterification of ME (Est-ME). For the preparation of the esterified adduct, the above preparation procedure was followed to prepare ME. This was then converted to Est-ME by the addition of 0.01 M BC to the hot adduct solution followed by continuous stirring for 4 h.[24] The solid product was washed with chlorobenzene several times and dried under vacuum.

2.2.3. Preparation of Ziegler−Natta Catalysts (Ti/ME and Ti/Est-ME). The final Ziegler−Natta catalysts were prepared by a general procedure reported in innumerable patents with the following modifications.[24,25] A suspension of Est-ME (100 mg) was stirred in chlorobenzene (22 mL) for 1 h at 110 °C as $TiCl_4$ (22 mL, 0.2 mol) was added over the course of 10 min. The resulting solid was filtered hot and washed for 10 min each with two 10 mL portions of $TiCl_4$ at 110 °C and filtered again followed by several washes with hexane at 60 °C to remove surface or physisorbed Ti species. Washing continued until the supernatant liquid did not show detectable levels of titanium alkoxide. Then the catalyst (Ti/Est-ME) was dried and stored in dry N_2 atmosphere. Similarly, the ME supported final catalyst (Ti/ME) was prepared.

2.3. Ethylene Polymerization. Ethylene polymerization was carried out in a Buchi glasuster glass polyclave reactor fitted with a thermocouple, an automatic temperature control unit, and a stirring speed of 500 rpm. In a typical polymerization, 0.5 L of dry hexane was added to the reactor at 75 °C, followed by TEAL (9% solution in *n*-hexane), and the catalyst was introduced into the reactor under a stream of dry N_2 and then evacuated. Ethylene (5 bar) was then fed at a constant pressure. Polymerization was carried out for 1 h at 75 °C.

2.4. Characterization Techniques. XRD patterns were recorded on a Rigaku Geiger flux instrument equipped with Ni-filtered Cu Kα radiation (λ = 1.5405 Å).[26] All molecular adducts and titanated catalysts were protected with a thin layer of nujol or handled strictly under dry N_2 atmosphere to avoid any degradation due to interaction with atmospheric components. Optical microscopic images of these adducts were recorded on an Olympus make (BX50, Japan) optical microscope. Triblock copolymer and toluene were added to the adduct, and the resultant solution was sonicated for 10 min to get a uniform dispersion. A thin liquid layer from the above solution was employed for recording images, mainly to avoid particle agglomeration. The morphology of the catalyst was examined by an environmental scanning electron microscopy (SEM) technique. A high-resolution FEI QUANTA 200 3D SEM was used to measure the surface morphology.[27] The catalyst samples were preserved under vacuum conditions. Voltage and the working distance varied during the measurements as noted on the SEM images. The surface area of the catalysts was determined by a Brunauer−Emmett−Teller (BET) method via nitrogen adsorption on NOVA 1200 Quanta Chrome equipment. Samples were handled and packed to the analysis tubes under a dry nitrogen atmosphere.[28] Thermal analysis of these adducts was recorded on Perkin-Elmer Diamond's thermogravimetry (TG) and differential thermal analysis (DTA) with alumina as the internal standard. Infrared spectral measurements were performed on a Rigaku IR spectrometer with nujol mull and KBr pellets.[29] Raman spectra were recorded on a Horiba JY Lab RAM HR 800 spectrometer excited with 633 nm lasers. While recording Raman measurements, to avoid any degradation of materials, a low-temperature setup (Linkam−Examine−THMS 600 setup connected to a TP94 temperature programmer and LN94 unit to cool the stage below ambient temperature using liquid nitrogen) was employed.[30] Sample temperature was maintained below 0 °C to avoid any degradation from atmospheric moisture.

The solid-state NMR experiments were carried out on a Bruker AVANCE 300 wide bore spectrometer equipped with a superconducting magnet with a field of 7.1 T using a 4 mm double resonance magic angle spinning (MAS) probe.[25,31] The operating frequencies for ^1H and ^{13}C were 300 and 75.4 MHz, respectively. The samples were packed into a 4 mm zirconia rotor and loaded into a Bruker's 4 mm MAS probe and spun about the magic angle (54.74°) at 8/10 kHz. The 90° pulses for proton and carbon were 2.6 (∼96 kHz) and 3.0 (∼83 kHz), respectively. The ^1H radio frequency (rf) field strength for heteronuclear two-pulse phase modulation (TPPM) decoupling was carried out at 100 kHz.[32] All single-pulse excitation (SPE) experiments were done using a 30° flip angle and with a recycle delay of 5/20 s, and cross-polarization (CP) experiments were performed using a recycle delay of 3 s and a contact time of 2.5 ms using a standard ramp-CP pulse sequence with the RF power 83 kHz.[33] All the chemical shifts were referenced to TMS by using adamantine as an external standard. Typically, 128−2048 scans were collected depending on the sensitivity of the sample.

3. RESULTS AND DISCUSSION

3.1. Powder X-ray Diffraction. Figure 1 shows the XRD patterns of anhydrous $MgCl_2$, ME and Est-ME, and Ti/ME and

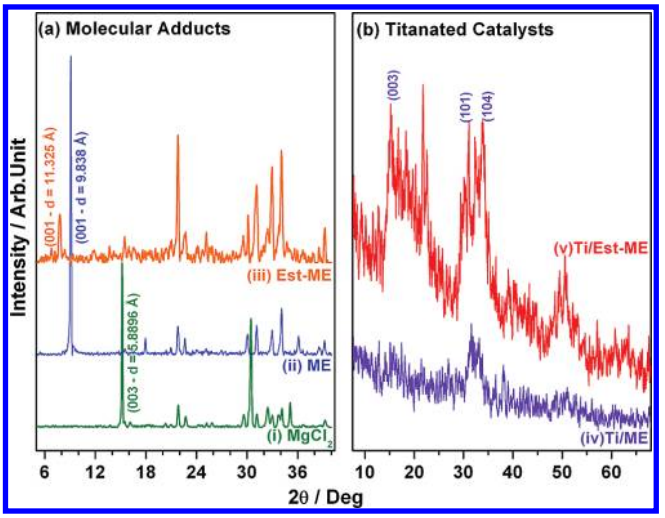

Figure 1. XRD patterns of (a) molecular adducts (ME and Est-ME) compared with anhydrous $MgCl_2$ and (b) final titanated catalyst supported on the ME and Est-ME molecular adducts (Ti/ME and Ti/Est-ME). (i) $MgCl_2$, (ii) (b) $MgCl_2 \cdot 6EtOH$ (ME), (iii) $MgCl_2 \cdot 5EtOH \cdot EtOCOPh$ (Est-ME), (iv) titanated ME (Ti/ME), and (v) titanated Est-ME (Ti/Est-ME).

Ti/Est-ME. Anhydrous $MgCl_2$ exhibits the cubic close packing with rhombohedral structure giving a strong XRD pattern at $2\theta = 35°$ (004) and 15.1° (003). However, the XRD pattern of the adducts varies depending on the amount of alcohol in $MgCl_2$.[34,35] The XRD pattern of ME shows a high intensity and characteristic (001) reflection at $2\theta = 9°$.[35−41] It is to be noted that the azeotropic distillation method[24,25] employed to prepare the above adducts leads to preferential (00z) plane oriented ME crystallites. This result is in good agreement with results reported earlier, in which Mg^{2+} is surrounded octahedrally by six ethanol molecules.[25,36] The XRD pattern of the esterified adduct shows a characteristic low-angle peak at 7.8° and hence an increase in the d-value of the (001) plane. This low-angle peak characterizes the esterified molecular adduct formation indicating the ester formation that occurs along the z-axis of ME. Indeed, this is the preferred route due to the lowest steric hindrance along the z-axis of the layered structure of $MgCl_2$.

After treatment of these adducts with $TiCl_4$, characteristic peaks for the molecular adduct disappear in the catalyst, and it shows broad diffraction features between 15 and 23°, 29 and 34°, and 49 and 51° corresponding to structurally disordered δ-$MgCl_2$. The low-angle peak observed below 10° for ME and Est-ME disappears, indicating a likely removal of EtOH molecules upon titanation; the same has been confirmed by solid state NMR, and it will be discussed later. The diffraction feature at about 16° is due to the stacking of −Cl−Mg−Cl− triple layers ((003) plane) along the crystallographic direction. Signals at 29−34° (101/104) and 49−51° are also related to stacking faults in the triple layers.[34,42] The growth of $MgCl_2$ crystal was terminated by the surface incorporated $TiCl_4$ and the ethyl benzoate ester coordinated, leading to assemblies of fine $MgCl_2$ crystallites that could be identified by the characteristic broad peaks in XRD analysis (Figure 1b). Furthermore, the incorporated $TiCl_4$ would be located on the surface of $MgCl_2$ leading to effective formation of the active species.

3.2. Surface Morphology Studies. Figure 2 shows the optical microscope image of the esterified adducts. Particles were homogeneously distributed and are of similar size. The particles

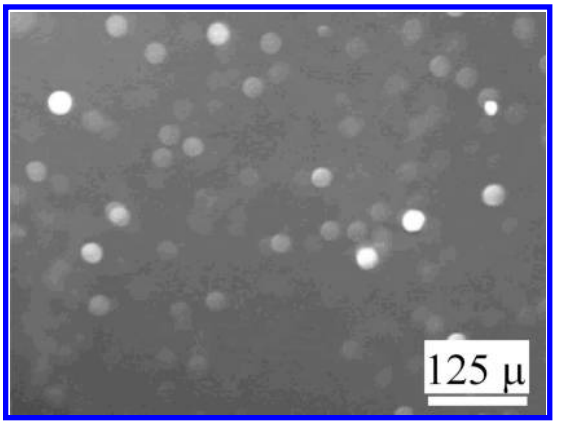

Figure 2. Optical microscopy image of esterified adducts (Est-ME) with uniform spherical morphology and a diameter around 25−30 μm.

are perfectly spherical in shape with a diameter of about 25−30 μm. None of the particles were agglomerated due to the employment of triblock copolymer.

Figure 3 shows the SEM photograph of (a) ME, (b) Est-ME, (c) Ti/ME, and (d) Ti/Est-ME, respectively. The SEM photographs shown in Figure 3 clearly show the spherical shape of both these adducts and catalysts. However, there are some changes on the surface of the support. First of all, the particle size has reduced drastically from 20 to 40 μm on pure adducts (Figures 3a and b) to less than 10 μm on titanated catalysts (Figures 3c and d). Apparently, smooth surfaces of the pure adducts become significantly porous upon titanation. The porous structure of the titanated catalysts is attributed to the removal of ethanol molecules from pure adducts, and this allows the creation of pores as well as the incorporation of $TiCl_3$ on the surface and pores. Particle size estimated on pure adducts from SEM (20−40 μm) is in correspondence with that of optical microscopy (25−30 μm).

3.3. Thermal Analysis. Figure 4 shows the results from TG/DTA of (a) ME, (b) Est-ME, (c) Ti/ME, and (d) Ti/Est-ME. The sample temperature was ramped from ambient to 300 °C at a rate of 10 °C/min under the flow of ultrahigh pure nitrogen (99.999%) at 40 mL/min. The well-defined weight loss and sharp DTA peaks indicate a systematic dissociation of ethanol molecules from the ME and Est-ME adducts. In the case of ethanol adducts, the first ethanol molecule dissociates around the boiling point of liquid ethanol at 68 °C (weight loss from 100 to 88%) followed by sequential dissociation of the remaining five-ethanol molecule (weight loss from 88 to 27%). The EtOH/$MgCl_2$ ratio was also identified to be 6 from the weight loss of the ME adduct due to the loss of EtOH molecules. In the case of the esterified adduct, the first ethanol molecule dissociates at 89 °C (weight loss from 100 to 90%), indicating the stronger binding force between EtOH and $MgCl_2$ in Est-ME. Indeed, the weight loss trend observed is significantly slower up to 130 °C with the Est-ME adduct compared to ME, again highlighting that EtOH is bound relatively stronger in the former.

However, between 130 and 245 °C, the remaining four-ethanol molecule dissociates. Weight loss in Est-ME corresponds to the dissociation of five EtOH molecules in total. No weight loss was observed >245 °C, and it is reasonable to assume that $MgCl_2$ with one molecule of ester remains >245 °C.

Thermal analysis of titanated catalysts (Figure 4b) also shows weight loss, and in particular DTA shows profound changes. There is no weight loss observed below 100 °C for both titanated

dx.doi.org/10.1021/jp1078289 |J. Phys. Chem. C 2011, 115, 1952–1960

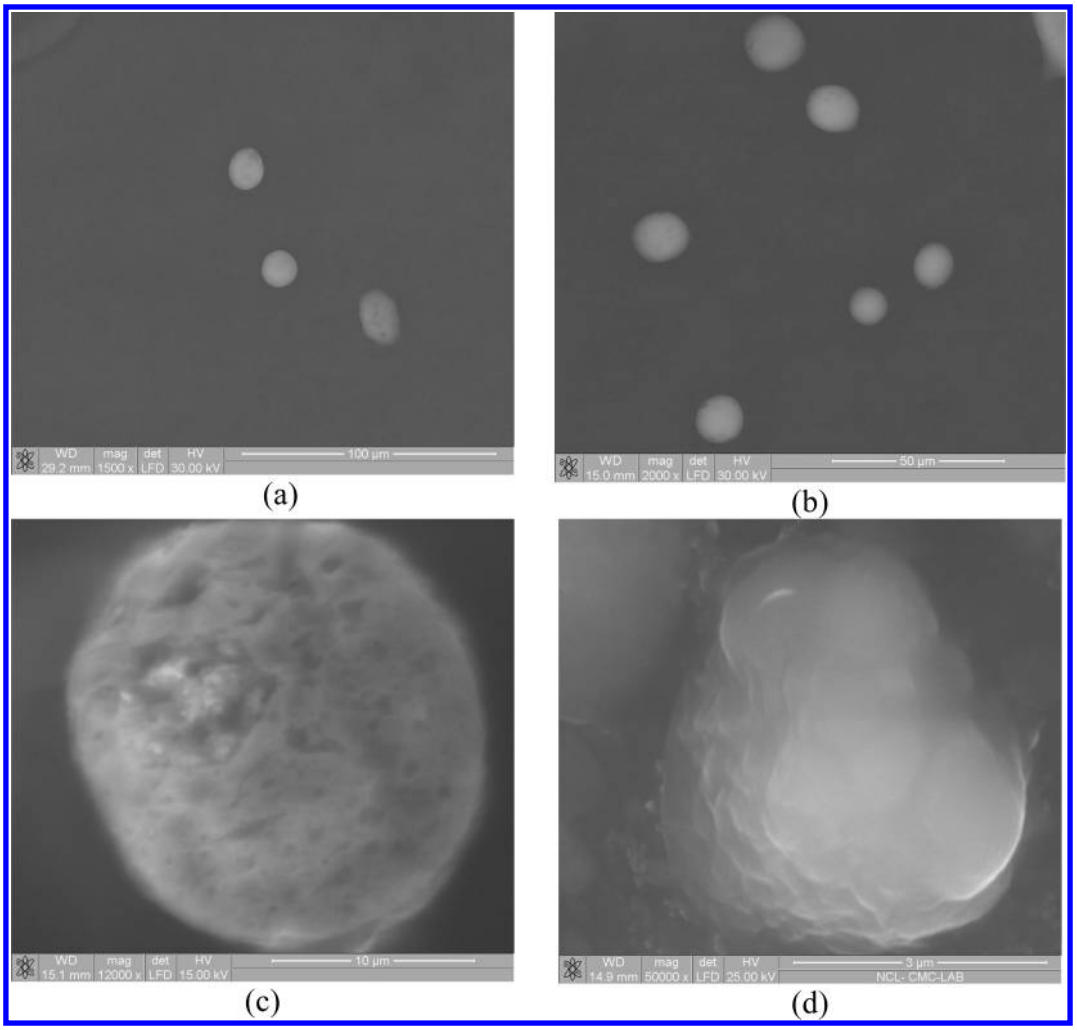

Figure 3. SEM images of molecular adduct, (a) ME and (b) Est-ME, and final titanated catalysts, (c) Ti/ME and (d) Ti/Est-ME. Scale bar is 200, 50, 10, and 3 μm for a, b, c, and d, respectively.

catalysts indicating a substantial removal of ethanol from the above catalysts. Nonetheless, weight loss observed above 100 °C may be attributed to the loss of any ethanol, trapped chlorinated ethers, and other solvent molecules from Ti/ME. Similarly, the weight loss observed between 130 and 250 °C from Ti/Est-ME might be due to desorption of various trapped components, like chlorinated ethers and solvent molecules. The presence of chlorinated ethers and solvent molecules has been supported by NMR data, which will be discussed later.

3.4. IR Spectroscopy. IR spectra of ME, Est-ME, BC, Ti/ME, and Ti/Est-ME are given in Figure 5. Adducts, such as ME and Est-ME, show that the absorption band at 3450 cm^{-1} is due to O−H stretching. High intense peaks observed at 2980−2900 cm^{-1} and 1500−1300 cm^{-1} for all samples are due to C−H stretching of nujol. Ethyl benzoate (EB) (liq.) displays the $\nu_{C=O}$ peak at 1720−1730 cm^{-1} (result not shown), while BC shows the ν_{OC-Cl} peak at 1780 cm^{-1} in addition to the above. Indeed, the Est-ME adduct shows the $\nu_{C=O}$ feature at 1730 cm^{-1} directly supporting the ester formation.[43] The esterified adduct shows $C-O-C_{str}$ and $O-C=O_{asym}$ signals at 1167 and 1106 cm^{-1}, respectively.

Similar to Est-ME, Ti/Est-ME also shows the $\nu_{C=O}$ peak, however, at 1680 cm^{-1}. This observation demonstrates that the ester part in Est-ME is strongly coordinated to $MgCl_2$ and cannot be removed by various steps involved in the catalyst preparation. However, the $\nu_{C=O}$ of ester shifts from 1730 cm^{-1} on Est-ME to 1680 cm^{-1} on Ti/Est-ME due to the changes in the electronic environment around the support material. Loss of ethanol molecules from Est-ME as well as coordination by the ester to $TiCl_3/TiCl_4$ in Ti/Est-ME are the possible reasons for the above shift in $\nu_{C=O}$.

3.5. Raman Spectroscopy. Figure 6 shows the Raman spectra of anhydrous $MgCl_2$, ethanol (liquid), ME, Est-ME, and EB (liq.). Raman spectra of $MgCl_2$ show a high intense peak at 243 cm^{-1} which has been assigned to the A_{1g} breathing mode of the $MgCl_6$ octahedra in the lattice.[42,44] Crystalline $MgCl_2$ belongs to the rhombohedral structure with D_{3d} space group and has a layered structure. Mg^{2+} is in a distorted octahedral configuration coordinated to six chlorine anions. In the Raman spectra of liquid ethanol, a broad and weak OH phonon mode observed at 3400−3100 cm^{-1} is due to the intermolecular hydrogen bonding. For ethanol, peaks at 430, 886, 1052, 1270, and 1094 cm^{-1} correspond to Raman modes associated with δ(CCO), symmetric CCO, antisymmetric CCO, CH_2 twist + δ(COH), and CO stretch + CH_3 rock + δ (COH) modes, respectively.[45] After the adduct formation with $MgCl_2$, ME shows one extra peak at 684 cm^{-1} in addition to the features of liquid ethanol mentioned above. The above Raman mode at 684 cm^{-1} is due to the formation of the characteristic

dx.doi.org/10.1021/jp1078289 |J. Phys. Chem. C 2011, 115, 1952–1960

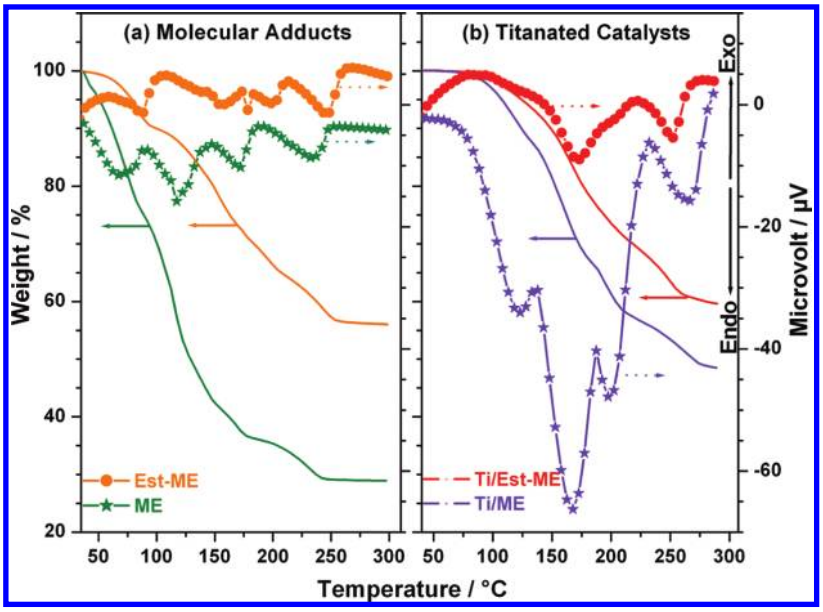

Figure 4. TG-DTA analysis of (a) ME and Est-ME molecular adducts and (b) final titanated catalysts, namely, Ti/ME and Ti/Est-ME.

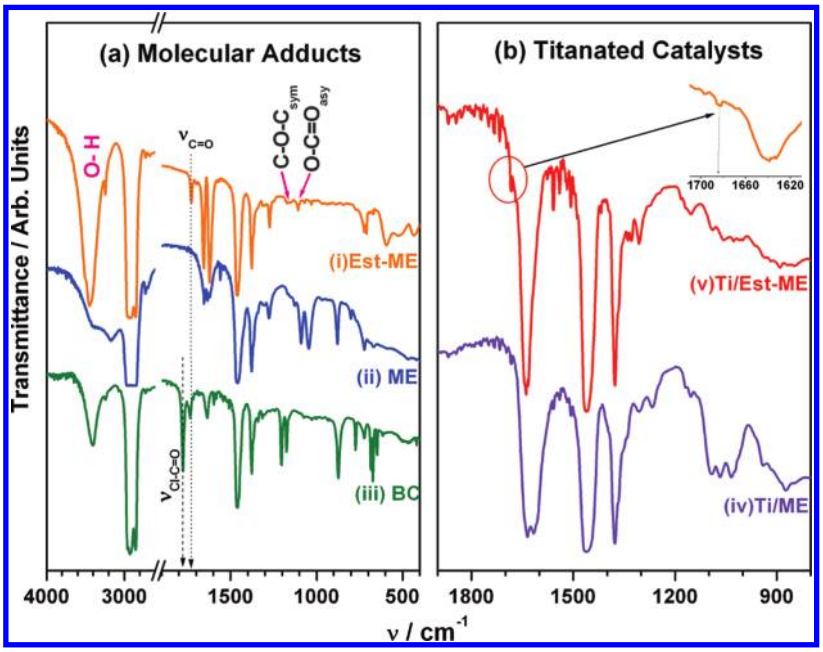

Figure 5. IR spectra of (a) molecular adducts, (i) ME and (ii) Est-ME and (iii) BC, and (b) titanated catalysts, (iv) Ti/ME and (v) Ti/Est-ME. Strong C−H vibrational features around 3000 and 1500 cm^{-1} are due to nujol. Ester formation in Est-ME is supported by the observation of the carbonyl feature at 1730 cm^{-1}, and the same is retained after titanation, albeit with a shift on Ti/Est-ME.

MgO_6 octahedron, and underscores the formation of the Mg−O bond between Mg and alcoholic oxygen.[42,46] In the case of esterified adduct, the Mg−O phonon mode shifted to a little higher value of 700 cm^{-1} which is due to the presence of the aromatic ester moiety in the adduct. This is in good agreement with TG/DTA results discussed earlier. In the Raman spectrum of liq. EB, the C═O breathing mode appears at 1717 cm^{-1} (results not shown); however, the C═O breathing mode of Est-ME shifted to 1703 cm^{-1} due to the coordination with $MgCl_2$. A shift in the Raman features of Est-ME, compared to ME, also underscores the changes in the structural and electronic environment.

3.6. Solid-State NMR Spectroscopy. The ^{13}C CP/MAS spectra of (a) ME, (b) Est-ME, (c) Ti/ME, and (d) Ti/Est-ME are shown in Figure 7. ^{13}C CP/MAS of the ME adduct exhibits two sharp peaks: the peaks at 58.9 and 17.6 ppm correspond to $-\underline{C}H_2OH$ and methyl carbon, respectively. The ^1H MAS spectrum of the ME adduct shows sharp peaks at 5.4, 3.6, and 1 ppm corresponding to $-O\underline{H}$, $-C\underline{H}_2-$, and $C\underline{H}_3$ protons, respectively (Figure 8). The sharpness of the peaks is due to the high mobility of the ethanol molecules in the highly symmetrical environment.[38−41] Formation of the esterified adduct was further supported by solid-state NMR. The presence of the peak at ∼169 ppm is due to the carbonyl carbon of the ester group. From the ^{13}C SPE-MAS spectrum, it is confirmed that only one ethanol out of six is converted to the corresponding ester. The ^1H MAS spectrum of

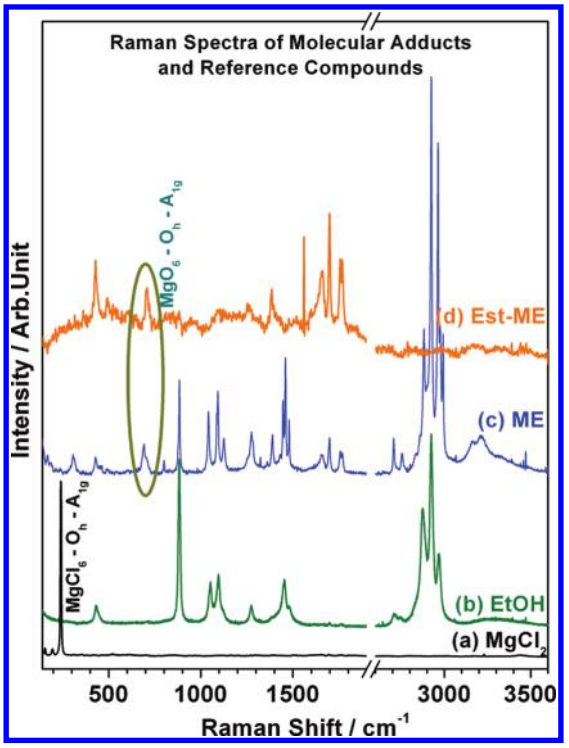

Figure 6. Raman spectra of standard compounds, (a) $MgCl_2$ and (b) ethanol, and molecular adducts, namely, (c) ME and (d) Est-ME.

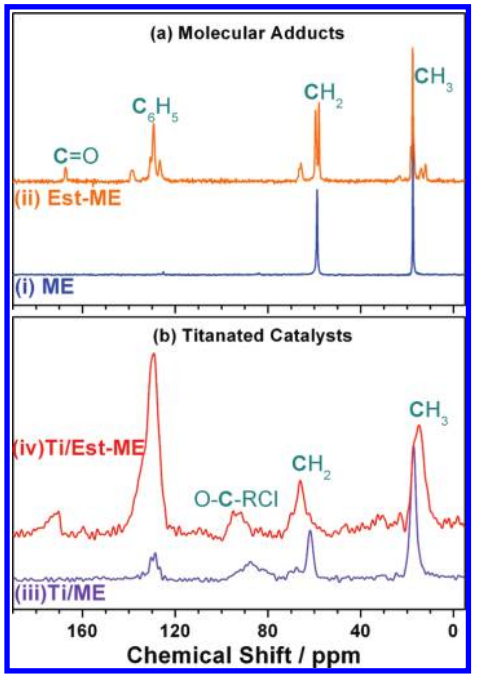

Figure 7. ^{13}C CP-MAS NMR spectra of (a) molecular adducts, (i) ME and (ii) Est-ME, and (b) titanated catalysts, (iii) Ti/ME and (iv) Ti/Est-ME.

Est-ME (Figure 8a) clearly shows the presence of aromatic protons, and the peaks are broader than that of the ME adduct, which indicates that the mobility as well as the symmetry are low after esterification.

The presence of the ester as IED in the final catalyst (Ti/Est-ME) was confirmed from the ^{13}C CP/MAS spectra shown in Figure 7b. As expected, various steps involved in the final catalyst

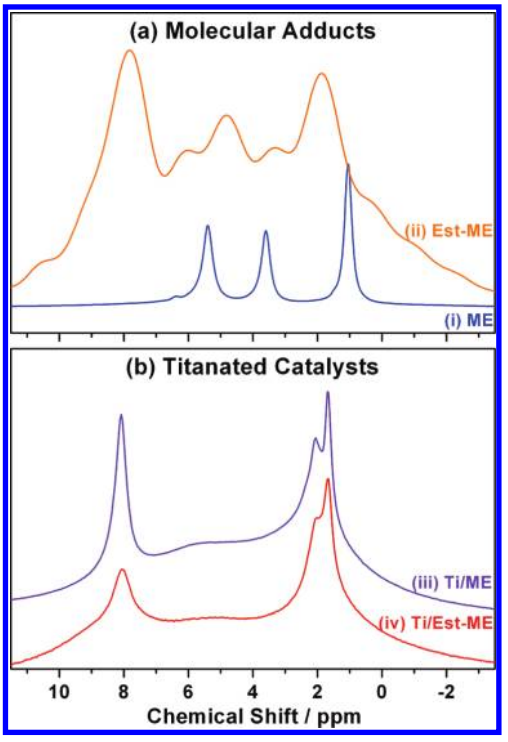

Figure 8. ^{1}H MAS spectra of (a) molecular adducts, (i) ME and (ii) Est-ME, and (b) titanated catalysts, (iii) Ti/ME and (iv) Ti/Est-ME.

preparation did not remove the ester group from the support, and the carbonyl carbon in the ester group appears at ~170 ppm. ^{13}C CP/MAS spectra of Ti/Est-ME and Ti/ME show an additional peak at 94 and 87.6 ppm, respectively. This may be due to the formation of small amounts of chlorinated ether. The reactions between ME or Est-ME with $TiCl_4$ produces HCl, which in turn leads to the formation of chlorinated ethers. The latter remains trapped within the pores of the support and could be observed by ^{13}C CP/MAS NMR; weight loss in TG-DTA also corresponds to the loss of chlorinated ether molecules (see Figure 4b). The ^{1}H MAS spectrum of Ti/ME and Ti/Est-ME catalysts show very sharp peaks at 8 and 2.5−1.6 ppm (Figure 8b) corresponding to protons from aromatic and ethyl species and chlorinated ethers, respectively.

3.7. Textural Characteristics. Table 1 shows the BET surface area and pore volume of adducts and titanated catalysts. It is to be mentioned here that the surface area of as-prepared molecular adducts shows a negligible value of 1−2 m^2/g. Apart from the much less porosity of molecular adducts, they could not be degassed (before surface area measurement) at temperatures higher than 40 °C as it would lead to loss of ethanol molecules. Surface area and pore size distribution measured through nitrogen adsorption isotherms on titanated catalysts are shown in Figure 9. Ti/ME and Ti/Est-ME show significantly high surface area (Table 1). However, the surface area of Ti/Est-ME is low due to the presence of ester. Indeed, the high surface area of Ti/ME is likely due to the removal of all EtOH molecules and hence the creation of high porosity. Roughly, a third of the porosity is retained with Ti/Est-ME (compared to Ti/ME) indicating the presence of ester molecules in the final catalyst. A careful analysis of adsorption isotherms indicates type II and IV (H3) adsorption isotherms for Ti/Est-ME and Ti/ME, respectively. An exponential increase in nitrogen adsorption observed for both catalysts at $P/P_0 \geq 0.8$ is to be noted. This is attributed to the presence of

dx.doi.org/10.1021/jp1078289 |J. Phys. Chem. C 2011, 115, 1952–1960

Table 1. Textural Characteristics of Molecular Adducts and Titanated Catalysts

material	particle morphology	surface area (m^2/g)	pore diameter (nm)	pore volume (cc/g)
Ti/ME	spherical	55.4	3.9	0.085
Ti/Est-ME	spherical	22.2	4.1	0.046
ME	spherical	1	~0.0	~0.0
Est-ME	spherical	2	~0.0	~0.0

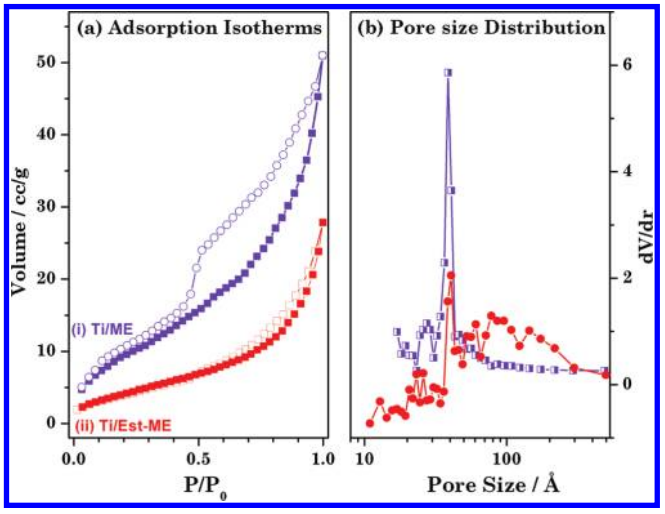

Figure 9. (a) Adsorption isotherms and (b) pore-size distribution of titanated catalysts.

Table 2. Titanation of $MgCl_2$-Based Adducts and Their Performance Evaluation for Ethylene Polymerization

catalyst	wt % of Ti	catalyst qty (mmol of Ti)	TEAL/Ti ratio	PE yield (g/g of catalyst)	PE yield (g/mmol of Ti)
Ti/ME	11	0.23	50	1300	572
Ti/Est-ME	11	0.23	20	1400	622

macropores in both the catalysts, particularly with slit-type pores. The difference observed in adsorption isotherms between the above two catalysts is to be noted. Indeed, the type II adsorption isotherm indicates an unrestricted monolayer−multilayer adsorption, which might be an important factor helping toward chain growth in polymerization.

3.8. Ethylene Polymerization. After the extensive characterization of molecular adduct and titanated catalyst, the activity of the catalyst was evaluated by ethylene polymerization (Table 2). Ethylene, rather than propylene, polymerization was chosen as the benchmark for comparing the activities of Est-ME and ME derived catalysts so that potential differences in energetics arising out of different orientations of propylene could be ignored. Indeed, DFT calculations on a model catalyst had shown that the energy differences between transition states corresponding to different orientations of propylene in the presence of IED could be substantial.[47] Ethylene polymerization was carried out with ME and Est-ME molecular adducts supported catalyst, as mentioned earlier, without any attempt to maximize the productivity by optimizing the experimental conditions. Triethyl aluminum (TEAL) was used as the cocatalyst. Higher yields (1400 g/g of catalyst) of polyethylene and productivity were obtained using Est-ME rather than the ME-supported catalyst (see Table 2). The increase in activity is about 9% and must be due to the presence of the coordinated ester moiety in the final Ti/Est-ME. Even though Ti/Est-ME exhibits lower surface area than that of Ti/ME, the higher activity must be attributed mainly to the presence of IED on the support. This also indicates that high surface area is not an absolute necessity for higher reactivity, and the right electronic environment of the final catalyst is an effective way[48] of enhancing its productivity for ethylene polymerization.

3.9. Genesis of Higher Activity of Ti/Est-ME. The detailed preparation, characterization by structural, spectroscopy, and microscopic analytical methods, and the evaluation of the titanated adducts for ethylene polymerization presented here provide some new information, especially on the molecular level properties and electronic structure of the molecular adducts and corresponding Ziegler−Natta catalysts. Although similar information has already been available in the literature,[6−23] they are derived from the analysis of polymer product and hence in an indirect manner. The four pieces of direct evidence from our work in support of the idea that IED enhances the activity come from (a) IED's existence in the final catalysts by all the characterization methods employed, in spite of several steps involved in the preparation; (b) significant changes in vibrational features in IR and Raman studies of Ti/Est-ME compared to the virgin adducts highlighting a stronger interaction between Ti^{3+}/Ti^{4+} in the adduct through the carbonyl group of IED; (c) higher polymerization activity observed with Ti/Est-ME compared to Ti/ME; and (d) higher activity of Ti/Est-ME at the cost of loss of surface area and pore volume compared to that of Ti/ME (Table 1). Although it is known that surface area generally increases the activity of catalysts, an increase in activity at the cost of textural properties underscores the origin of higher activity and is not due to textural properties or any preferred orientation of final catalysts. This is also further supported by weak diffraction features of Ti/Est-ME, as preferred orientation generally leads to higher intensity of XRD features. Nonetheless, some contribution from any of the particular crystallite facets cannot be ruled out at this stage, as studies such as high-resolution TEM (HRTEM) might be necessary to confirm that. Our attempts to measure surface crysallinity by HRTEM studies were not successful due to the amorphous nature of Ti/Est-ME and big particle sizes. It is unlikely that any preferred orientation of crystallites is present in Ti/Est-ME. Titanation of Est-ME introduces Ti on the surfaces of the adduct and its coordination with the ester group, leading to broader peaks in XRD (Figure 1b). Hence, from the above discussion and our earlier work on other catalytic systems,[26,48] it is clear that the genesis of enhanced catalytic activity in the present case is best attributed to electronic interactions rather than other factors. Ti^{2+} is known to be inactive for polymerization, while partial reduction of $Ti^{4+/3+}$ to Ti^{2+} in a side reaction with TEAL is one of the main catalyst deactivation pathways. The coordination of IED to $Ti^{4+/3+}$ probably makes the active sites less susceptible to such deactivation than those in Ti/ME.

4. CONCLUSIONS

We report on the preparation of $MgCl_2$-based adducts, namely, ME, Est-ME, and their corresponding titanated Ziegler−Natta catalysts. In situ esterification of ME with BC leads to an adduct with a coordinatively bound internal electron donor to $MgCl_2$. Structural, spectroscopic, textural, and microscopic studies

of these adducts and final catalysts have been thoroughly investigated by many techniques. XRD studies indicate the structural changes due to ester formation in Est-ME, and this adduct maintains the rhombohedral structure of $MgCl_2$. IR, Raman, and solid-state NMR show the characteristic signal for the ester moiety. An optical microscopy image shows that the morphology of adducts is perfectly spherical with a diameter between 25 and 30 μm. The XRD study of the final titanated catalysts shows the presence of structurally disordered δ-$MgCl_2$. IR and ^{13}C CP/MAS NMR data of Ti/Est-ME clearly indicate the existence of the ester moiety, even though the Est-ME support is titanated with $TiCl_4$. Significant changes observed in spectroscopic analysis of the ester moiety from a simple adduct to titanated catalysts highlight the changes in its electronic environment. Polymerization of ethylene using the Ziegler−Natta catalyst supported on the esterified $MgCl_2$ adduct shows more activity compared to the Ti/ME adduct which is also high compared to the free $MgCl_2$ supported Ziegler−Natta catalyst. In spite of lower surface area, better polymerization activity associated with Ti/Est-ME than Ti/ME highlights the significance of the right electronic environment rather than textural characteristics. The present study motivates the preparation of such novel catalysts with complex alcohols in the future. Further work on this catalyst and its role in controlling stereospecificity is our future work.

AUTHOR INFORMATION

Corresponding Author

*E-mail: cs.gopinath@ncl.res.in. www.ncl.org.in/csgopinath. Fax: 0091-20-2590 2633. Dr. Bhaduri's e-mail: s-bhaduri@northwestern.edu.

ACKNOWLEDGMENT

We thank Dr. Raksh Vir Jasra and Dr. Ajit Mathur for their continuous support. We thank Mr. Viralkumar Patel for experimental assistance during catalyst preparation, characterization, and ethylene polymerization. SEG thanks CSIR, New Delhi, for a senior research fellowship. We thank Reliance Industries Limited, Mumbai, India, for financial support.

REFERENCES

(1) Albizzati, E.; Giannini, U.; Collina, G.; Noristi, L.; Resconi, L. In *Polypropylene Handbook: Polymerization, Characterization, Properties, Applications*; Moore, E. P., Ed.; Hanser Publ., Jr.:NY, 1996; p 11.

(2) Luciani, L.; Kashiwa, N.; Barb, P. C.; Toyota, A. Ger. 2643143, Montedison and Mitsui Petrochemical, invs. *Chem. Abstr.* **1977,** *87,* 68893v.

(3) Albizzati, E.; Cecchin, G.; Chadwick, J. C.; Collina, G.; Giannini, U.; Morini, G.; Noristi, L.; Resconi, L. In *Polypropylene handbook,* 2nd ed.; Pasquini, N., Ed.; Carl Hanser Verlag: Munich, 2005; Chapter 2.

(4) Chadwick, J. C. *Macromol. Symp.* **2001,** *173,* 21.

(5) Cecchin, G.; Morini, G.; Pelliconi, A. *Macromol. Symp.* **2001,** *173,* 195.

(6) Sergeev, S. A.; Bukatov, G. D.; Zakharov, V. A.; Moroz, E. M. *Makromol. Chem.* **1983,** *184,* 2421.

(7) Terano, M.; Kataoka, T.; Keii, T. In *Catalytic polymerization of olefins*; Keii, T., Soga, K., Eds.; Kodansha-Elsevier: Amsterdam, 1986; p 407.

(8) Sormunen, P.; Hjertberg, T.; Iiskola, E. *Makromol. Chem.* **1990,** *191,* 2663.

(9) Terano, M.; Saito, M.; Kataoka, T. *Makromol. Chem. Rapid Commun.* **1992,** *13,* 103.

(10) Busico, V.; Corradini, P.; De Martino, L.; Proto, A.; Savino, V.; Albizzati, E. *Makromol. Chem.* **1985,** *186,* 1279.

(11) Sacchi, M. C.; Tritto, I.; Shan, C.; Mendichi, R.; Noristi, L. *Macromolecules* **1990,** *24,* 6823.

(12) Ribour, D.; Monteil, V.; Spitz, R. *J. Polym. Sci., Part A: Polym. Chem.* **2008,** *46,* 5461.

(13) Boulif, A.; Lonër, D. J. *J. Appl. Crystallogr.* **1991,** *24,* 287.

(14) Metz, G.; Wu, X.; Smith, O. S. *J. Magn. Reson. A* **1994,** *110,* 219.

(15) Andoni, A.; Chadwick, J. C.; Niemantsverdriet, J. W.; Thüne, P. C. *J. Catal.* **2008,** *257,* 81.

(16) Soga, K.; Shiono, T.; Doi, Y. *Makromol. Chem.* **1988,** *189,* 1531.

(17) Sacchi, M. C.; Forlini, F.; Tritto, I.; Locatelli, P.; Morini, G.; Baruzzi, G.; Albizzati, E. *Macromol. Symp.* **1995,** *89,* 91.

(18) Busico, V.; Corradini, P.; Martino, L. D.; Proto, A.; Albizzati, E. *Makromol. Chem.* **1986,** *187,* 1115.

(19) Busico, V.; Corradini, P.; Martino, L. D.; Proto, A.; Savino, V.; Albizzati, E. *Makromol. Chem.* **1985,** *186,* 1279.

(20) Sacchi, M. C.; Tritto, I.; Locatelli, P. *Prog. Polym. Sci.* **1991,** *16,* 331.

(21) Barbe, P. C.; Cecchin, G.; Noristi, L. *Adv. Polym. Sci.* **1987,** *81,* 1.

(22) Noristi, L.; Barbè, P. C.; Baruzzi, G. *Macromol. Chem.* **1995,** *192,* 115.

(23) Kashiwa, N.; Kojoh, S. *Macromol. Symp.* **1995,** *89,* 27.

(24) Bhaduri, S.; Gupta, V. K. U.S. Patent 6841633, 2005.

(25) Thushara, K. S.; Mathew, R.; Ajithkumar, T. G.; Rajamohanan, P. R.; Bhaduri, S.; Gopinath, C. S. *J. Phys. Chem. C* **2009,** *113,* 8556.

(26) Shiju, N. R.; Anilkumar, M.; Mirajkar, S. P.; Gopinath, C. S.; Satyanarayana, C. V.; Rao, B. S. *J. Catal.* **2005,** *230,* 484.

(27) (a) Mapa, M.; Kumarsrinivasan, S.; Bhange, D. S.; Saha, B.; Chakraborty, P.; Viswanath, A. K.; Gopinath, C. S. *Chem. Mater.* **2010,** *22,* 565. (b) Mapa, M.; Gopinath, C. S. *Chem. Mater.* **2009,** *21,* 351.

(28) Vijayaraj, M.; Gopinath, C. S. *J. Catal.* **2006,** *241,* 83.

(29) (a) Mathew, T.; Vijayaraj, M.; Pai, S.; Tope, B. B.; Hegde, S. G.; Rao, B. S.; Gopinath, C. S. *J. Catal.* **2004,** *227,* 175. (b) Mathew, T.; Tope, B. B.; Shiju, N. R.; Hegde, S. G.; Rao, B. S.; Gopinath, C. S. *Phys. Chem. Chem. Phys.* **2002,** *4,* 4260. (c) Waghmode, S.; Vetrivel, R.; Hegde, S. G.; Gopinath, C. S.; Sivasanker, S. *J. Phys. Chem. B* **2003,** *107,* 8517.

(30) Mapa, M.; Thushara, K. S.; Saha, B.; Chakraborty, P.; Janet, C. M.; Viswanath, R. P.; Madhavan Nair, C.; Murty, K. V. G. K.; Gopinath, C. S. *Chem. Mater.* **2009,** *21,* 2973.

(31) (a) Maity, N.; Rajamohanan, P. R.; Ganapathy, S.; Gopinath, C. S.; Bhaduri, S.; Lahiri, G. K. *J. Phys. Chem. C* **2008,** *112,* 9428. (b) Maity, N.; Basu, S.; Mapa, M.; Rajamohanan, P. R.; Ganapathy, S.; Gopinath, C. S.; Bhaduri, S.; Lahiri, G. K. *J. Catal.* **2006,** *242,* 332.

(32) Bennett, A. E.; Rienstra, C. M.; Auger, M.; Lakshmi, K. V.; Griffin, R. G. *J. Chem. Phys.* **1995,** *103,* 6951.

(33) Metz, G.; Wu, X.; Smith, O. S. *J. Magn. Reson. A* **1994,** *110,* 219.

(34) Sobota, P. *Coord. Chem. Rev.* **2004,** *248,* 1047.

(35) Bart, C. J. *J. Mater. Sci.* **1995,** *30,* 2809.

(36) Valle, G.; Baruzzi, G.; Paganetto, G.; Depaolit, G.; Zannetti, R.; Marigo, A. *Inorg. Chim. Acta* **1989,** *156,* 157.

(37) Sozzani, P.; Bracco, S.; Comotti, A.; Simonutti, R.; Camurati, I. *J. Am. Chem. Soc.* **2003,** *125,* 12881.

(38) Magalhase, D. N. T.; Filho, O. D. C.; Coutinho, F. M. B. *Eur. Polym. J.* **1991,** *27,* 827.

(39) Forte, M. C.; Coutinho, F. M. B. *Eur. Polym. J.* **1996,** *32,* 223.

(40) Xu, R.; Liu, D.; Wang, S.; Wang, N.; Mao, B. *J. Mol. Catal. A* **2007,** *263,* 86.

(41) Ye, Z.-Y.; Wang, L.; Feng, L.-F.; Gu, X.-P.; Chen, H.-H.; Zhang, P.-Y.; Pan, J.; Jiang, S.; Feng, L.-X. *J. Polym. Sci., Part A: Polym. Chem.* **2002,** *40,* 3112.

(42) Tewell, C. R.; Malizia, F.; Ager, J. W., III; Somorjai, G. A. *J. Phys. Chem. B* **2002,** *106,* 2946.

(43) Jeong, Y.; Lee, D. *Makromol. Chem.* **1990,** *191,* 1487.

(44) Balasubrahmanyam, K. *J. Chem. Phys.* **1966,** *44,* 3270.

(45) Dollish, F. R.; Fateley, W. G.; Bentley, F. *Characteristic Raman Frequencies of Organic Compounds*; Wiley-Interscience: New York, 1974; p 443.

(46) Rönkkö, H.-L.; Knuuttila, H.; Denifl, P.; Leinonen, T.; Venäläinen, T. *J. Mol. Catal. A: Chem.* **2007,** *278*, 127.
(47) Mukhopadhyay, S.; Kulkarni, S. A.; Bhaduri, S. *J. Organomet. Chem.* **2005,** *690*, 1356.
(48) (a) Sivaranjani, K.; Gopinath, C. S., *J. Mater. Chem.*, DOI: 10.1039/C0JM03825C.(b) Naik, B.; Parida, K. M.; Gopinath, C. S. *J. Phys. Chem. C* **2010,** *114*, 19473. (c) Sathish, M; Viswanathan, B.; Viswanath, R. P.; Gopinath, C. S. *Chem. Mater.* **2005,** *17*, 6349. (d) Gholap, S.; Badiger, M. V.; Gopinath, C. S. *J. Phys. Chem. B* **2005,** *109*, 13941. (e) Mathew, T.; Shylesh, S.; Devassy, B. M.; Satyanarayana, C. V. V.; Rao, B. S.; Gopinath, C. S. *Appl. Catal., A* **2004,** *273*, 35. (f) Velu, S.; Suzuki, K.; Gopinath, C. S.; Hattori, T.; Yoshida, H. *Phys. Chem. Chem. Phys.* **2002,** *4*, 4260. (g) Satyanarayana Reddy, A.; Gopinath, C. S.; Chilukuri, S. V. *J. Catal.* **2006,** *243*, 278.